Synergistic enhancement of properties in copper oxide-reinforced polystyrene nanocomposites via in situ polymerization

R. Anju[1] · M. T. Ramesan[1]

Abstract
The study primarily focuses on the in situ synthesis of polystyrene (PS) and copper oxide (CuO) nanocomposites. An extensive analysis was conducted on the optical, thermal, mechanical, and electrical properties of PS with different CuO concentrations. The effective inclusion of CuO into PS was characterized by Fourier-transform infrared spectroscopy (FTIR), UV–visible spectroscopy, filed emission scanning electron microscopy (FE-SEM), X-ray diffractometry (XRD), differential scanning calorimetric analysis (DSC) and thermal gravimetric analysis (TGA). The reinforcement of CuO into the PS was established through FTIR. The optical bandgap energy deduced from UV–visible spectra decreases with CuO addition, whereas the refractive index rises significantly with the addition of CuO nanoparticles up to 7 mass%. The XRD analysis revealed the amorphous to crystalline transformation of PS with the homogeneous dispersion of nanoparticles. The SEM–EDX analysis revealed the uniform distribution of CuO nanofillers in the PS matrix. The CuO addition considerably increased the glass transition temperature and thermal stability of PS. The tensile strength, impact resistance and hardness of nanocomposite were significantly increased with the loading of CuO in the polymer matrix. The AC conductivity and dielectric constant of the PS was improved with the addition of CuO nanoparticles. The effect of temperature on conductivity, activation energy, and pre-exponential factor was determined using the universal power law and the Arrhenius equation. The highest electrical and mechanical properties were observed for 7 mass% nanocomposite. The synthesized PS/CuO nanocomposites with excellent optical characteristics, thermal stability, electrical conductivity, dielectric constant and mechanical strength can be used in supercapacitors and flexible nano-electronic devices.

Keywords Polystyrene · Copper oxide · Nanocomposites · Mechanical properties · Electrical properties · Thermal properties

Introduction

The development of polymer nanocomposites in recent years has brought new technology and advantageous opportunities to business and society at large. The formation of a nanocomposite by dispersing nanoscale fillers into a polymer matrix has generated significant interest due to the enhanced mechanical, thermal, and electrical properties it can provide [1–3]. The nanocomposites offer superior characteristics than the parent material. These nanocomposites have shown promising applications in various industries, such as automotive, aerospace, electronics, and packaging [4–6]. Additionally, the ability to tailor the properties of nanocomposites by controlling the type, size, and concentration of fillers has further fuelled their widespread adoption in different sectors [7]. There are different methods that have been reported for the synthesis of polymer nanocomposites such as in situ polymerization, emulsion polymerization, sol–gel reactions, and melt processing [8, 9]. The interactions between the nanoparticles and polymer matrix determine the characteristics of the synthesized nanocomposites. Poor nanofiller–matrix interactions lead to poor composite properties. The in situ polymerization process can be utilized to get around this restriction. This method involves the simultaneous formation of the polymer matrix and the dispersion of the nanofillers within it, leading to a more homogeneous distribution and stronger bonding between the two components [10]. Moreover, in situ polymerization allows

✉ M. T. Ramesan
mtramesan@uoc.ac.in

[1] Department of Chemistry, Centre for Polymer Science and Technology, University of Calicut, Calicut University P.O, Malappuram, Kerala 673 635, India

for better control over the size, shape, and orientation of the nanofillers, further enhancing the properties of the nanocomposites [11]. Thus, nanocomposites generated by the in situ polymerization method have enhanced mechanical properties compared to those prepared by solution compounding or melt mixing procedures [12].

Metal oxides have significant technological implications due to their ability to generate charge carriers, great chemical stability and affordable cost [13, 14]. Their unique structural and surface properties allow for precise control over their size, shape, and surface chemistry, further enhancing their potential for tailored applications. CuO [15], CeO$_2$ [16], ZnO [17], TiO$_2$ [18], Fe$_3$O$_4$ [19], NiO [20], etc., are the most commonly used metal oxide nanoparticles. They act as good fillers for polymer matrix due to their satisfying optical, electrical, mechanical, and antimicrobial properties. CuO nanoparticles have unique optical, thermal and electronic properties, widely used as optoelectronic devices, solar cells, high-tech superconductors, photoconductive and photothermal applications, ceramic resistors, etc. [21].

Polystyrene is an amorphous thermoplastic polymer with good transparency, dimensional stability, high rigidity, good electrical properties and low cost [22]. It is a good commercial polymer with wide applications in packaging, electronics, composites, construction and other areas. At the same time, polystyrene has a brittle nature, poor chemical resistance, a relatively low melting point, weak impact resistance, low flexibility, poor scratch resistance, etc. [23]. In this regard, the addition of nanofillers will result in the property enhancement of polystyrene. The thermal degradation of polystyrene-zinc oxide nanocomposites was done by Motawie et al. [24]. Similarly, Castro et al. studied the photoacoustic properties of polystyrene/Pd/TiO$_2$ nanocomposites [6]. According to the literature reviews, no in-depth research has been done to improve the mechanical, electrical, optical and thermal properties of polystyrene nanocomposites. In this regard, we have chosen polystyrene and CuO nanoparticles for the current investigation. In the current study, the thermal, optical, electrical, and mechanical characteristics of PS/CuO nanocomposites were systematically examined.

Materials and methods

Materials

Styrene, benzoyl peroxide, toluene, ethanol, copper sulphate, sodium hydroxide (purchased from Merk India) and deionized water were used throughout the experiment. Stabilizers present in styrene are removed using a 10% NaOH solution followed by distillation. All other reagents are of 99% purity and used without further purification.

Synthesis of copper oxide nanoparticles

The co-precipitation approach was used to prepare copper oxide nanoparticles with copper (II) sulphate as a metal precursor. 0.1 M copper sulphate solution was prepared by dissolving it in deionized water. 0.2 M NaOH solution was added dropwise into it, and the resulting black precipitates were washed several times with deionized water and ethanol till pH reached 7. The purified precipitates were dried, and finally, the precursors were calcined at 400 °C for 4 h.

Synthesis of polystyrene/CuO nanocomposites

Polystyrene/ CuO nanocomposites were synthesized via in situ polymerization of styrene with varying mass fractions (0, 3, 5, 7, and 10 mass%) of CuO. Initially, 5 g of purified styrene monomer was dissolved in toluene. CuO nanoparticles were dispersed in 25 mL toluene and mixed with the styrene monomer, and the mixture was stirred well and ultrasonicated for 20 min to produce a homogenous solution. Finally, 2.0 g benzoyl peroxide dissolved in 15 mL toluene was added to the above solution, and the polymerization reaction was carried out at 85 °C for 4 h in an inert atmosphere. The resulting product was isolated from the above reaction mixture by coagulating with excess methanol. The PS/CuO nanocomposite was finally dried in a vacuum oven at 60 °C for 24 h.

Instrumentation

The interactions between polystyrene and copper oxide nanoparticles were analysed by FTIR spectroscopy. The studies were carried out using the JASCO 4100 FTIR spectrometer in the region 400–4000 cm^{-1}. Potassium bromide tablet method was used for the sample preparation. The XRD analysis of PS/CuO nanocomposites was carried out by a Rigaku D/MAX 2200 Model X-ray Diffractometer using Cu Kα ($\lambda = 1.5407$Å) radiation. The experiment was conducted at a scanning rate of 2.0° min^{-1} and a 2θ range from 0 to 90°. The UV–visible absorption spectra of PS and its nanocomposites with different loadings of CuO nanoparticles were recorded using a JASCO V-770 spectrophotometer. The bandgap energy of PS/CuO nanocomposites was determined by Tauc plot. The surface analysis of the nanocomposites was done using (FE-SEM, Carl Zeiss [Germany] VP-500 model) field-emission scanning electron microscopy. The thermal stability of the PS and nanocomposites was analysed using a Hitachi STA7200 thermogravimetric analyser. The samples were heated from ambient temperature to 700 °C in an inert environment at a heating rate of 10 °C min^{-1}. The glass transition temperature (T$_g$) of PS/CuO nanocomposites

was analysed by Shimadzu DSC-50 differential scanning calorimetry. A sample of 8–10 mg was weighed and placed in an aluminium pan. It was heated from room temperature to 250 °C at a heating rate of 10 °C min⁻¹. The tensile strength was carried out on UTM G-410B with maximum load of 5 kN at a speed of 2 mm min⁻¹ at 25 °C as per the ASTM D 638. The Zwik 5102 impact-testing device was used to assess impact strength. Using ASTM D2240, the Shore D hardness of the polymer nanocomposites was calculated. Eight readings were collected for each sample in different spots, and the average reading was reported. The Hioki impedance analyser (HIOKI 3570 model) was used to measure the electrical resistivity and dielectric characteristics of the nanocomposites over a frequency range of 100–1 MHz. The analysis was performed at varying temperatures (30, 50, 70 and 90 °C).

Results and discussion

FTIR spectra

The FTIR spectra of CuO, PS and PS/CuO nanocomposites are shown in Fig. 1. The characteristic IR peaks of CuO nanoparticles are obtained at 607, 515 cm⁻¹. The spectra of PS exhibit absorption peaks at 3075 and 3033 cm⁻¹ due to aromatic C–H stretching vibration. The peak obtained at 1604, 1498, and 1456 cm⁻¹ corresponds to aromatic C=C stretching vibration in the PS matrix. The existence of benzene ring is indicated by these peaks. The C–H out-of-plane bending vibration in PS is represented by the peaks at 795 and 652 cm⁻¹. This confirms that there is only one substituent in the benzene ring. The absorption bands at 2928
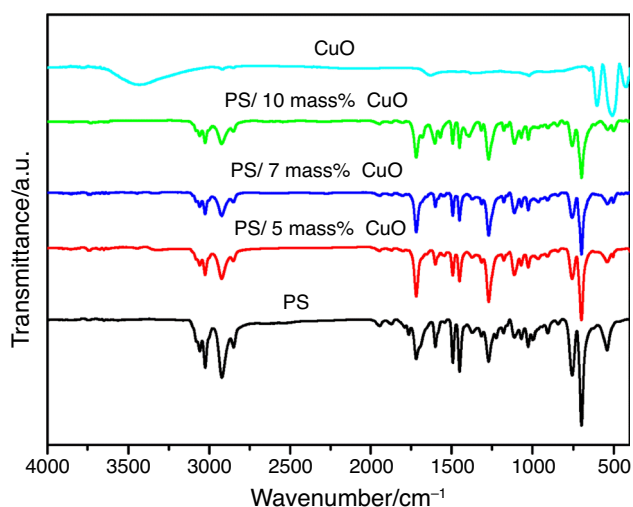
and 2850 cm⁻¹ show the existence of methylene groups [25, 26]. The IR spectra of PS/CuO nanocomposites exhibit the characteristic absorption peaks of PS with the formation of nanoparticles at 505 cm⁻¹, confirming the presence of CuO bond in the polymer matrix. Moreover, the aromatic C–H stretching vibration peaks are slightly shifted to 3069 and 3026 cm⁻¹ as compared to the spectra of PS. Similarly, the C–H out-of-plane bending vibration is also shifted to 762 and 699 cm⁻¹.

UV–visible spectroscopy

The UV–visible spectra of PS and its CuO nanocomposites are displayed in Fig. 2. The prominent absorption peak of PS at 252 nm, which is associated with the π-π* transition, is caused by forbidden transitions in the excited states of the polymer. The figure clearly shows that the nanocomposites' UV peak has shifted slightly to the right (from 252–258 nm). The UV absorption peaks of the nanocomposites appear to be broader to those of pure PS. This redshift and broadening of the absorption peaks in the nanocomposites imply that the addition of CuO nanoparticles to the polymer matrix causes an increase in structural disorder or aggregation, which results in a wider range of permitted electronic transitions. This effect may be explained by interactions between the polymer chains and the CuO nanoparticles, which alter the electronic properties of the nanocomposites. The intensity of the absorption peaks of the nanocomposites is increasing with the loading of CuO nanoparticles. Maximum intensity and broadness are observed for 7 mass% nanocomposite. Beyond 7 mass%, the intensity decreases, and this is attributed to the particle agglomeration in the nanocomposites. Also, the nanocomposites do not show any UV absorbance
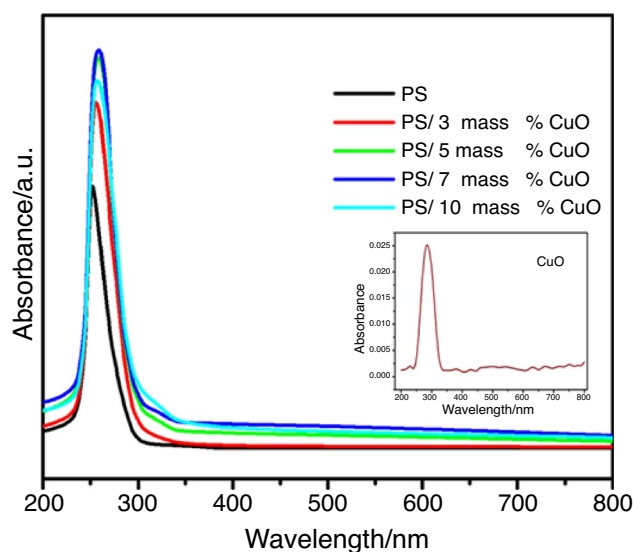

Fig. 1 FTIR spectra of CuO and CuO-incorporated PS nanocomposites

Fig. 2 UV–visible spectra of PS/CuO nanocomposites

behaviour above 400 nm. This indicates that the nanocomposites are transparent to UV radiation beyond the 400 nm range. This particular feature enables potential applications in a variety of industries, including optics and electronics, where UV protection is not necessary or desirable.

Optical bandgap energy

The study of the optical bandgap energy (E_g) provides significant insights into the electronic properties of PS/CuO nanocomposites. Figure 3 illustrates a graphic representation (Tauc plot) of these results, enabling a clear comparison of the bandgap energies across various compositions. The E_g values for PS and PS/CuO nanocomposites are calculated using the Tauc equation:

$$\alpha h\upsilon = \beta(h\upsilon - Eg)m \tag{1}$$

where α is the linear absorption coefficient, β a constant, h is the planks constant, $and\ \upsilon$ is the frequency of light. The exponent m is a constant that represents the optical absorption process. The nature of the energy gap or the transition involved is decided by the value of m. It can have values ½ and 2 for indirect allowed transition and direct allowed transitions, respectively. We have plotted $(\alpha hc/\lambda)^2$ against $h\upsilon$, photon energy. The optical bandgap energy is obtained by extrapolating the straight-line portion of the curve to $\alpha = 0$.

It is evident from the graphs that the band gap energy value drops with the addition of CuO nanoparticles. This results from an increase in the valence and conduction band shift [27]. The 7 mass% sample of these composites exhibit the lowest bandgap energy, possibly as a result of the effective distribution of CuO on PS at that loading. Above this loading, the bandgap energy value rises, possibly as a result of the aggregation of CuO particles in the polymer matrix.

The refractive index of PS/CuO nanocomposites can be calculated from the obtained E_g values using the equation

$$\frac{n^2 - 1}{n^2 + 2} = 1 - \sqrt{\frac{E_g}{20}} \tag{2}$$

Figure 4 illustrates the variation of E_g values and related refractive index with CuO nanoparticle loading. As the dopant concentration increased, the refractive index rose until 7 mass% sample, after which it started to fall. The increase in packing density of the PS/CuO nanocomposites suggested by the reference may be the cause of the refractive index increases with concentration. On the other hand, structural abnormalities at higher loading 10 mass% result in a decline in n values. Nanocomposites with higher refractive index values are excellent for optoelectronic and anti-reflective applications.

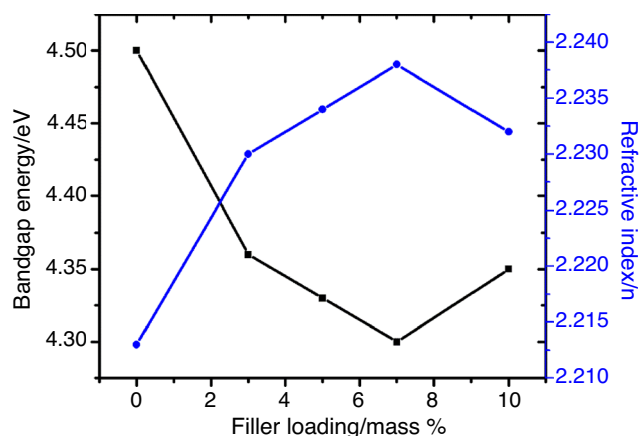**Fig. 3** Tauc plots of PS and PS/CuO nanocomposites
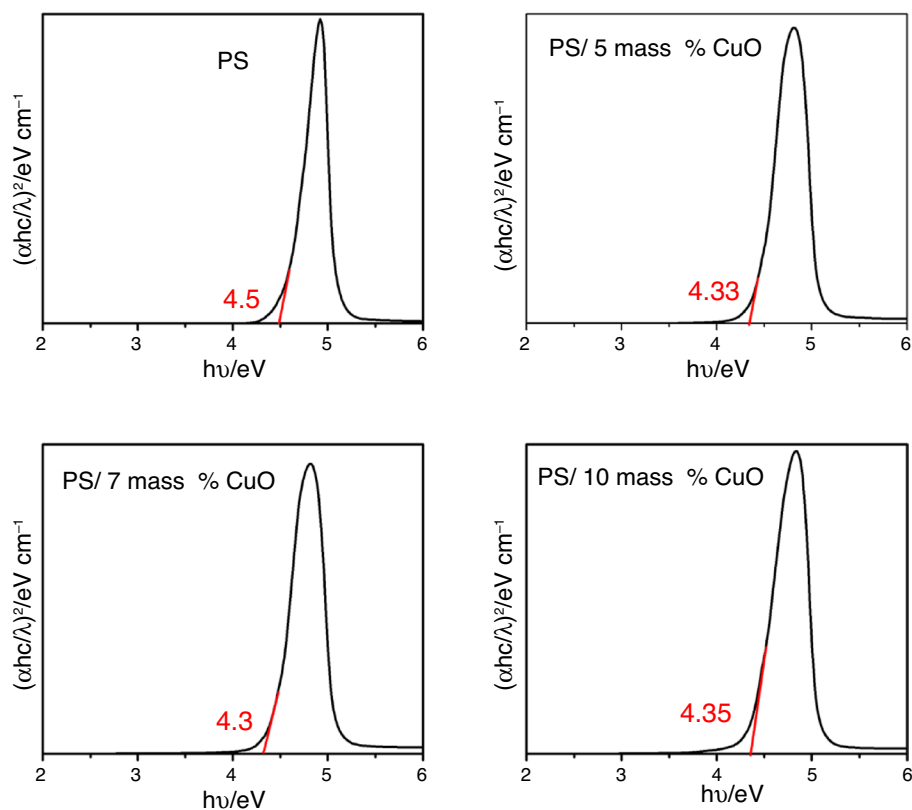
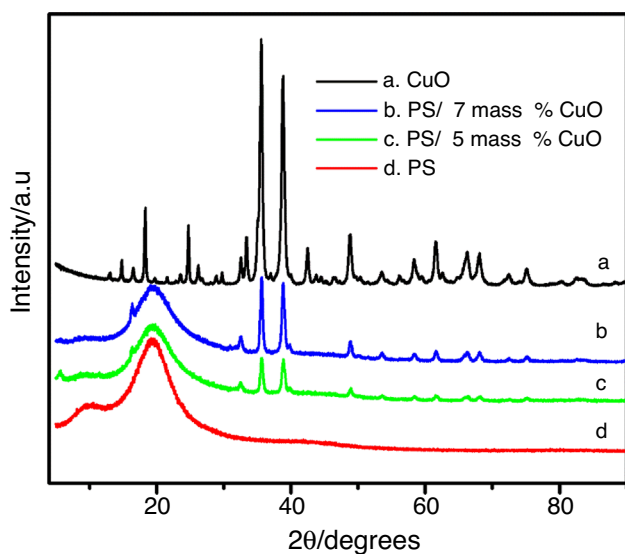**Fig. 4** Bandgap energy and refractive index of PS and PS/CuO nanocomposites

Fig. 5 XRD pattern of CuO nanoparticle and CuO-loaded PS

XRD analysis

The presence of CuO nanoparticles in the synthesized PS polymer nanocomposites was confirmed by the XRD analysis. Figure 5 shows the XRD patterns obtained for CuO nanoparticles, PS and PS nanocomposites. The XRD pattern of the synthesized CuO nanoparticle shows characteristic peaks at $2\theta = 18.3°$ (020), 24.5° (021), 32.4° (002), 33.16° (112) 35.53° (022), 38.47°(111), 42.29° (131), 48.89° (151) representing its crystalline nature [28]. The average crystalline size (D) of CuO nanoparticle is calculated using the Scherrer equation.

$$D = \frac{k\lambda}{\beta \cos \theta}, \tag{3}$$

where k is a dimension less shape factor ($=0.9$), λ is the wavelength of X-ray beam ($=1.54\text{Å}$ for CuKα), β is the line broadening at half maximum intensity (FWHM) in radians, and θ is the Bragg angle [50]. The average crystalline size obtained is ~ 34 nm. The amorphous character of PS is indicated by the broad peak found at $2\theta = 19.31°$ and a weak peak at $2\theta = 10.43°$ in the XRD pattern. It is found that the characteristic peaks of CuO nanoparticle appears in the XRD pattern of PS/CuO nanocomposites, and at the same time the weak peak at $2\theta = 10.43°$ is absent in PS/CuO nanocomposites. There is a decrease in the intensity and width of the amorphous peaks at $2\theta = 19.31°$ is observed in nanocomposites. The intensity of CuO peaks in the nanocomposite pattern increased with filler loadings. All of these changes confirm the formation of nanocomposites and shows an increase in the crystallinity of the polymer reinforced with nanofiller.

FE-SEM–EDX analysis

The surface morphology of PS and PS/CuO nanocomposites, analysed by the FE-SEM, along with the EDX spectra for 7 and 10 mass% sample is shown in Fig. 6. The EDX spectrum of synthesized PS/CuO nanocomposites shows the presence of both copper and oxygen elements. The FE-SEM image of PS exhibits a homogeneous smooth surface, while the incorporation of nanoparticles changes the plane surface into a rough surface. CuO nanoparticles are observed to be homogeneously distributed within the PS matrix in the FE-SEM images. Among the nanocomposites 7 mass% loading exhibits more uniform dispersion of CuO nanoparticles. Since the 7 mass% sample possesses more effective and uniform dispersion of nanoparticles, the interfacial interaction between the nano CuO and PS matrix seemed to be enhanced. As the percentage composition increases the homogeneity of the nanofillers in the polymer matrix decreases and they begin to aggregate. At 10 mass% loading the CuO nanoparticles undergo self-agglomeration, which negatively affects their compatibility with the polymer matrix. This results in a reduced interfacial attraction between the polymer and nanofiller. Therefore, it may be inferred from FE-SEM images that the highest interfacial bonding is found in the 7 mass% nanocomposite, and it is supposed to show the best mechanical characteristics.

DSC analysis

Figure 7 displays the DSC curves of PS and its nanocomposites with different loadings of CuO. The glass

Fig. 6 FE-SEM image of PS with **a** 0, **b** 3 CuO, **c** 7 and **d** 10 mass% CuO along with the EDX spectra for the 7 mass% and 10 mass%
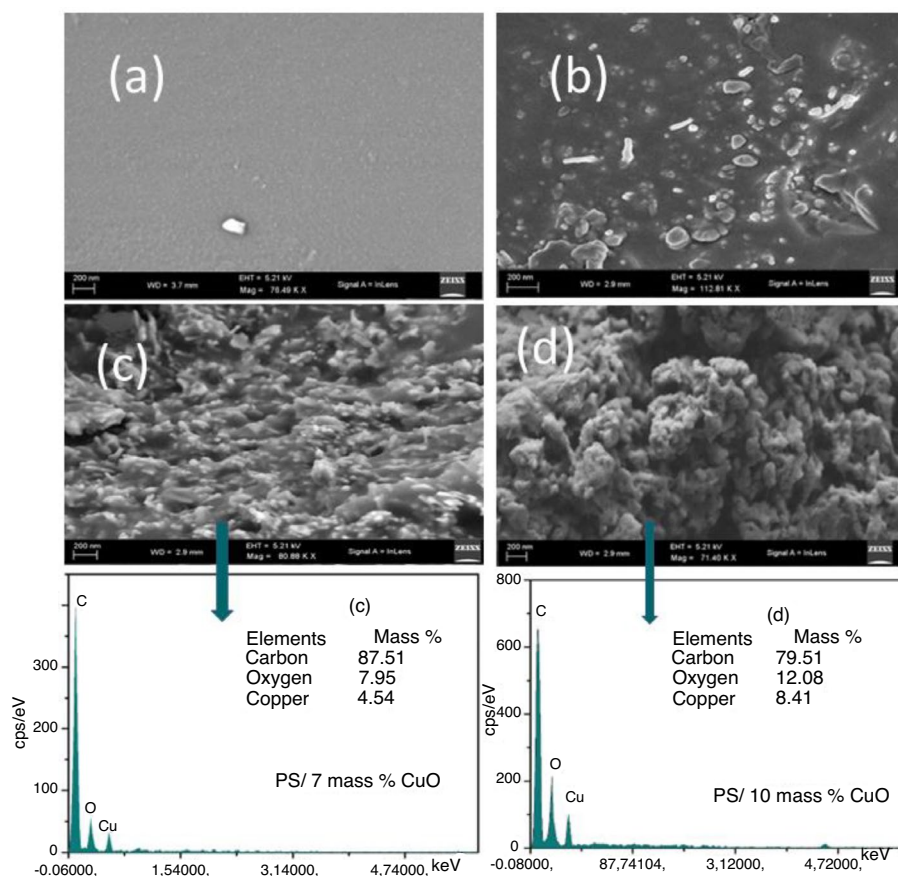
transition temperature, or the temperature at which the polymer transforms from a glassy state to a rubbery one, is responsible for a dramatic endothermic dip in the DSC curve. The glass transition temperature for pure PS and the 3, 7 and 10 mass% nanocomposites are observed at 124.7 °C, 132 °C, 134 °C, and 140 °C, respectively. The improved thermal stability of PS by the addition of CuO nanoparticles is evident from the DSC analysis. The XRD study has already shown that the PS/CuO nanocomposites have acquired a crystalline character. Therefore, the strong filler–polymer interaction and the constrained mobility of the molecular chains in the spaces between the scattered nanoparticles are to blame for the improved thermal stability of the polymer nanocomposites [29]. The acquired crystalline nature of the PS/CuO nanocomposites is already evident from the XRD analysis.

TGA

TGA was used to examine the thermal stability of PS and its nanocomposites with various loadings of CuO nanoparticles. The resultant TGA profiles are illustrated in Fig. 8. Pure PS and the nanocomposites follow single-phase degradation behaviour. It is clear from the TG analysis that the thermal stability of PS/CuO nanocomposites is higher than the parent PS.

Also, the thermal stability of nanocomposites further increases with the addition of CuO nanoparticles. The thermal degradation of pure PS is observed around 280 °C. This is due to the decomposition of polystyrene into the styrene monomer. At the same time, the degradation temperature of nanocomposites is raised to 350 °C. PS/10 mass% CuO shows the maximum thermal stability. This enhanced thermal stability exhibited by the nanocomposites is due to the presence of metal oxide nanoparticles in them. CuO nanoparticles prevent the mobility of PS, which prevents volatile compounds in the polymer matrix from degrading and thus improves the heat stability of PS composites. Moreover, the analysis of the char residue left at 600 °C for each sample further supports the thermal stability. The metal oxide nanoparticles in the polymer decreased the development of carbonaceous char layers, inhibiting the thermal decomposition process [29].

Mechanical properties

Tensile strength

Tensile strength is the capacity of a material to hold a mass while being stretched to a certain amount without breaking, and it is influenced mainly by the nature of the polymer matrix, the nanofillers used, the synthetic procedures and
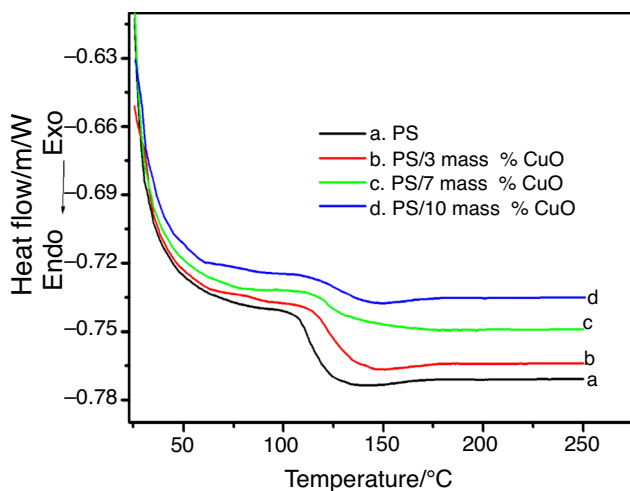
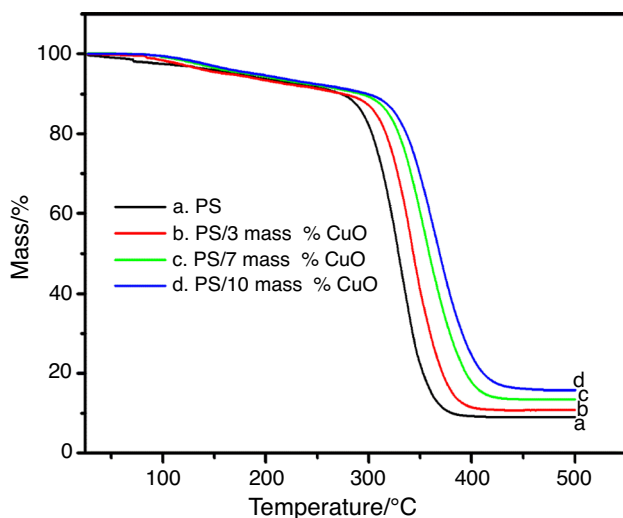**Fig. 7** DSC profile of PS with different loadings of CuO nanoparticles

Fig. 8 TGA of PS with various compositions of CuO

the extent of interaction [28]. Strong tensile mechanical strength is an important requirement for the commercial applications of polymer nanocomposites. Table 1 shows the impact of CuO nanoparticles on the tensile characteristics of PS. As we add more CuO nanoparticles, the tensile strength of polystyrene rises. PS/7 mass% CuO nanocomposite is found to have the highest tensile strength. About 40% of the increase in tensile strength is observed as compared to pure PS. The enhanced tensile strength of nanocomposites is a result of the insertion of nanoparticles, which enables the polymer matrix to sustain the stress created without rupturing [24]. The tensile strength slightly decreases with further loading of nanoparticles. 10 mass% nanocomposite shows decreased tensile strength. This is due to the aggregation of nanofillers in the polymer matrix and thereby diminishes

the filler–polymer interaction. The tensile modulus also follows the above trend. The modulus value increases with the addition of CuO nanoparticles up to a particular loading. The 7 mass% nanocomposite exhibits the maximum tensile modulus due to the homogeneous dispersion of nanoparticles. At higher loadings, the tensile modulus decreases due to decreased interfacial interaction.

Impact strength

Impact strength is a measurement of how much energy a material can hold when it is suddenly shattered. Low impact strength is a main disadvantage of polymers. So, enhancement of impact strength is necessary to broaden the application of nanocomposites. The particle size, the nature of the filler, the type of polymer, and the filler–matrix interactions will greatly influence the impact strength of polymer nanocomposites [30]. The impact strength of PS/CuO nanocomposites is listed in Table 1. As the CuO nanofiller loading increases, the impact strength of PS is increasing. PS/7 mass% CuO loading exhibits maximum impact strength. About a 60% enhancement in impact strength is observed for the 7 mass% nanocomposite. This is attributed to the effective incorporation of CuO nanoparticles in the PS matrix, which is already evident from XRD and SEM analysis. Thus, the polystyrene is well reinforced with CuO nanofiller. Beyond 7 mass% loading, the impact strength slightly decreases due to the increased brittleness of nanocomposites.

Hardness

The hardness of polymer nanocomposites was measured using shore durometer. The shore D hardness of PS and PS/CuO nanocomposites is displayed in Table 1. The hardness of polystyrene increases with the addition of CuO

Table 1 The mechanical properties of PS with different contents of CuO

Samples	Tensile strength/ MPa	Modulus/MPa	Impact strength/ KJ m^2	Hardness/ shore D
PS	29.13	500	12.41	42
PS/3 mass% CuO	32.81	522	14.21	43
PS/5 mass% CuO	35.68	546	16.75	44.5
PS/7 mass% CuO	39.96	556	19.26	46
PS/10 mass% CuO	37.45	550	18.45	48

nanoparticles. During the measurement of hardness, the polystyrene matrix contains CuO nanoparticles with a high degree of stiffness, which results in elevated levels of indentation resistance. The PS/10 mass% CuO nanocomposite exhibits the maximum hardness. About 16% of the enhancement in hardness is observed at this loading. The polymers with hardness value less than 65 are considered soft materials. Soft polymeric materials have flexible electronic applications and are also used in automotive applications [31].

AC conductivity at room temperature

The frequency-dependent ac electrical conductivity of PS and its CuO nanocomposites is demonstrated in Fig. 9. From the graph, it can be seen that for all samples, conductivity rises as applied frequency rises. The nonlinear increase in conductivity with frequency accounts for the existence of non-ohmic type conduction. Lower conductivities at lower frequencies are caused by insulating grain boundaries, and conducting grains are responsible for conductivity dispersions at higher frequencies [32]. The AC conductivity of PS is increased by the addition of CuO nanoparticles up to 7 mass% loadings, and after this mass%, a drop in conductivity is seen. This increase in the conductivity of nanocomposites in comparison with PS is due to the effective dispersion of CuO nanoparticles in the polymer matrix. The drop in conductivity above 7 mass% loadings of CuO nanoparticles can be due to the generation of agglomerates, which impede the flow of charge carriers. Agglomeration of nanoparticles reduces the effective surface area available for charge transport, which lowers conductivity.

Temperature-dependent AC conductivity

Figure 10 shows how the AC conductivity of PS and PS/CuO nanocomposites varies with frequencies at various temperatures. For all samples, the conductivity graphs increase linearly with frequency at all temperatures. It is evident from the plots that the AC conductivity of nanocomposites increases with temperature. The bipolar hopping mechanism refers to the movement of charge carriers between localized states, which becomes more prominent at low temperatures. On the other hand, at high temperatures, thermally induced polaron hopping occurs where charge carriers are able to move through the lattice by overcoming energy barriers. These distinct mechanisms contribute to the AC conductivity behaviour observed at different temperature ranges. The temperature-dependent conductivity is explained by the polaron hopping theory. This suggests that there are two kinds of polaron theories, big polaron (conductivity declines with frequency at all temperatures) and small polaron (conductivity rises with frequency at all temperatures). Here,
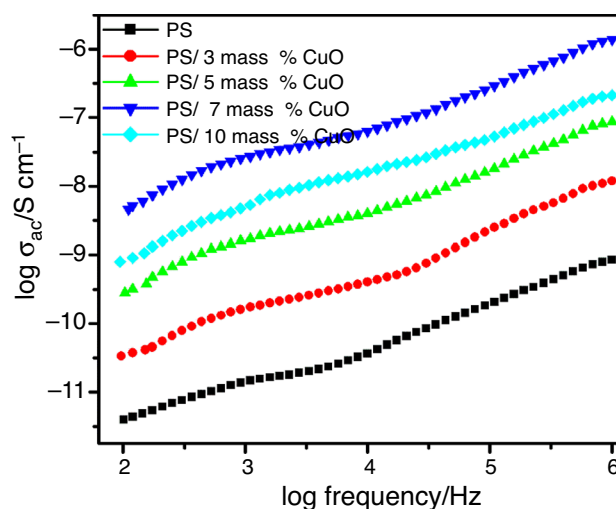
Fig. 9 AC conductivity of PS and its nanocomposites

small polaron theory is relevant in the case of PS/CuO nanocomposites at all temperatures.

The energy needed by ions to break through the potential barrier and flow freely is known as the activation energy (Ea). The activation energy at different frequency ranges is calculated from the slope of the Arrhenius plot:

$$\sigma_{ac} = \sigma_0 \exp^{(-Ea/kT)} \tag{4}$$

where σ_0, k and T are the pre-exponential factor, Boltzmann constant and absolute temperature, respectively [33]. The Arrhenius plot (log σ_{ac} vs. 1000/T) of PS and nanocomposites is displayed in Fig. 11, and the corresponding activation energy is listed in Table 2. Thermally enhanced hopping of charge carriers is evident from the linear nature of Arrhenius plots. The activation energy of the samples decreases with an increase in frequency and filler concentration due to this hopping. The lower activation energy at higher frequency indicates the increased conductivity of the samples. The activation energy decreases with the loading of nanoparticle up to 7 mass%. The PS/10 mass% CuO nanocomposite shows s slightly increased activation energy due to agglomeration of CuO nanoparticles.

Dielectric constant

The dielectric constant (ε') measures the ability of a material to store electrical energy in an electric field. Figures 12 and 13 show the frequency-dependent dielectric constants of pure PS and its nanocomposites at room temperature and various temperatures. Dielectric constant values are found to decrease exponentially with frequency. At lower

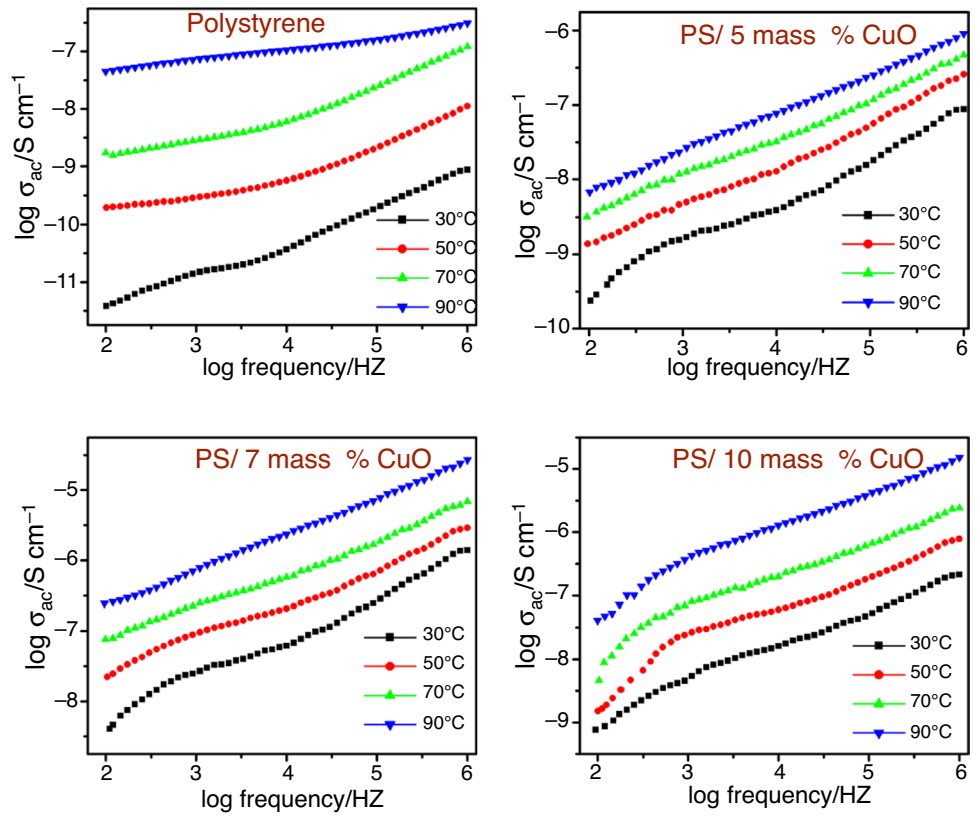**Fig. 10** The AC conductivity of PS and PS/CuO at various temperatures

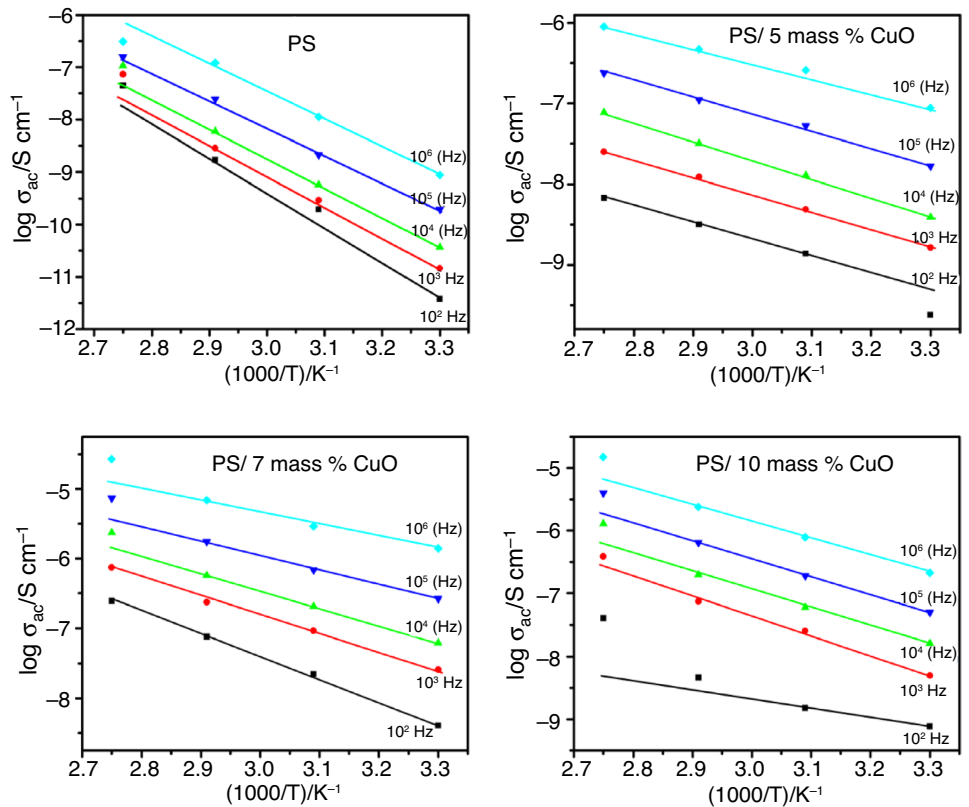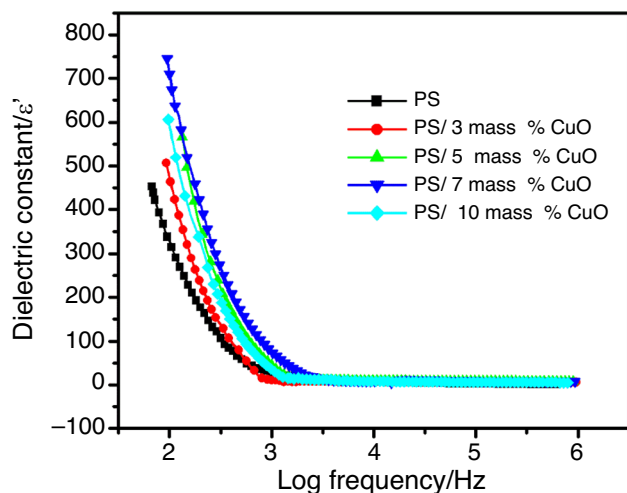**Fig. 11** Arrhenius plots for PS and PS/CuO nanocomposites

Table 2 Activation energy values of PS and PS/CuO nanocomposites at various frequencies

| samples	Activation energy/eV		
	10^4/Hz	10^6/Hz	10^6/Hz
PS	5.5089	5.2681	5.1778
PS/3 mass%CuO	5.4439	5.2175	4.9157
PS/5 mass%CuO	2.277	2.1710	1.8726
PS/7 mass%CuO	2.5041	2.0102	1.6866
PS/10 mass%CuO	2.8612	2.8784	2.6446

Fig. 12 Dielectric constant of PS and PS/CuO nanocomposites

frequencies, the dielectric constant values are relatively higher for all samples. At these frequencies, the dipoles present in the nanocomposites will orient themselves in the direction of applied field [9]. However, in higher frequency ranges, the electric field fluctuations are considerably quicker than the oscillating charge carriers, preventing them from aligning themselves in the applied field's direction. As a result, the dielectric constant value decreases

[33, 34]. PS/CuO nanocomposites exhibit a considerable increase in dielectric constants in lower frequency domains when compared to pure PS. This is in consistent with the space charge polarization between the components. The maximum (ε') value is observed for 7 mass% loaded nanocomposite which may be due to the uniform dispersion of CuO nanofiller into the polymer matrix. The variation of dielectric constant with temperature is depicted in Fig. 13. On increasing temperature, a greater number of free charge carriers attain sufficient energy and orient more frequently against the applied field, thus the (ε') value increases in the lower frequency region. At lower temperatures, the charge carrier polarization becomes less, which results in the lowering of dielectric constant values. Due to the lack of charge accumulations and interfacial polarization, the influence of temperature on the dielectric constant is minimal at higher frequencies [34].

Conclusion

Copper oxide nanoparticle-reinforced polystyrene nanocomposites were synthesized successfully by the single-step in situ free radical polymerization method, and their optical, thermal, mechanical, and temperature-dependent electrical properties were examined. The FTIR measurements revealed the attachment of CuO nanoparticles in the polystyrene matrix. The enhancement in crystalline nature with the addition of CuO nanoparticles in PS is demonstrated by the rise in the intensity of CuO peaks in the XRD pattern of nanocomposites. The significant red shift observed in the absorption spectra of PS nanocomposites strongly recommends the incorporation of CuO nanoparticles into polystyrene. The PS/7 mass% CuO nanocomposite has a lower bandgap energy and the maximum refractive index than the parent polystyrene due to the homogeneous dispersion of CuO. The SEM examination further supported the homogeneous nanoparticle dispersion in the 7 mass% nanocomposite. Due to the inclusion of CuO, the glass transition temperature of nanocomposites rose. The

Fig. 13 Variation of dielectric constant with frequency at different temperatures
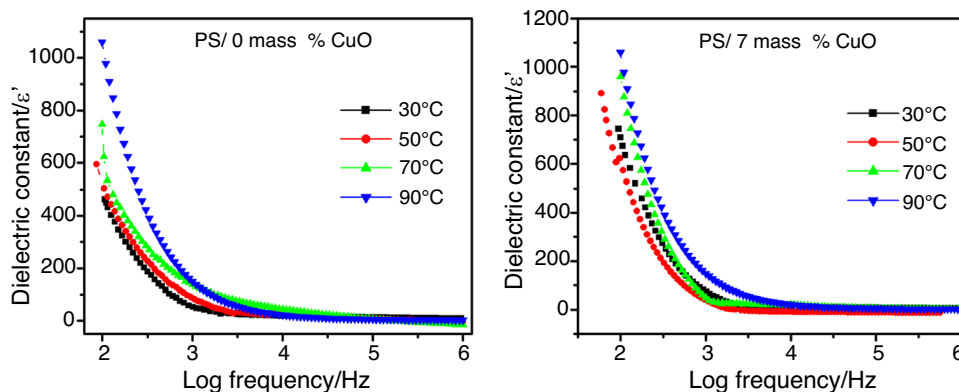
increase in T_g and thermal stability with the reinforcement of nanoparticle was clearly evinced from the DSC and TGA, respectively. The mechanical strength, modulus, hardness, and impact strength of the PS nanocomposites were greatly enhanced with the addition of nanoparticles. The 7 mass% nanocomposite showed excellent mechanical characteristics due to the effective reinforcement of nanoparticles. The AC conductivity and the dielectric constant increase with temperature, frequency, and filler concentration, and the activation energy decreases with the loading of CuO particles. PS/CuO nanocomposites have excellent mechanical properties, enhanced thermal properties, good optical properties, and enhanced conductive capabilities, making them suitable for application in optoelectronic devices and flexible conducting materials.

Declarations

References

1. Baatti A, Erchiqui F, Godard F, Bussières D, Bébin P. DMA analysis, thermal study and morphology of polymethylsilsesquioxane nanoparticles-reinforced HDPE nanocomposite. J Therm Anal Calorim. 2020;139:789–97. https://doi.org/10.1007/s10973-019-08497-x.

2. Khairy M, Amin NH, Kamal R. Optical and kinetics of thermal decomposition of PMMA/ZnO nanocomposites. J Therm Anal Calorim. 2017;128:1811–24. https://doi.org/10.1007/s10973-016-6062-x.

3. Parvathi K, Verma M, Ramesan MT. Enhanced thermal, electrical and mechanical properties of nickel oxide reinforced chlorinated natural rubber/poly (indole) blend nanocomposites. J Therm Anal Calorim. 2023;148:10139–49. https://doi.org/10.1007/s10973-023-12358-z.

4. Indolia AP, Gaur MS. Investigation of structural and thermal characteristics of PVDF/ZnO nanocomposites. J Therm Anal Calorim. 2013;113:821–30. https://doi.org/10.1007/s10973-012-2834-0.

5. Mathen JJ, Madhavan J, Thomas A, Edakkara AJ, Sebastian J, Joseph GP. Transparent ZnO–PVA binary composite for UV-A photo detector: optical, electrical and thermal properties followed by laser induced fluorescence. J Mater Sci Mater Electron. 2017;28:7190–203. https://doi.org/10.1007/s10854-017-6400-1.

6. Castro MF, Triviño GC, Morales J, Visurraga JD, Contreras CC. Synthesis and study of photoacoustic properties of (Pd/TiO$_2$)/polystyrene nanocomposites. Polym Bull. 2009;62:355–66. https://doi.org/10.1007/s00289-008-0024-9.

7. Mohammadsalih ZG, Inkson BJ, Chen B. Structure and properties of polystyrene-co-acrylonitrile/graphene oxide nanocomposites. J Compos Sci. 2023;7:225. https://doi.org/10.3390/jcs7060225.

8. Zafar MF, Siddiqui MA. Preparation and characterization of natural fiber filled polystyrene composite using in situ polymerisation technique. Adv Mater Process Technol. 2020;8:169–79. https://doi.org/10.1080/2374068X.2020.1798087.

9. Suhailath K, Ramesan MT. Investigations on the structural, mechanical, thermal, and electrical properties of Ce-doped TiO$_2$/poly(n-butyl methacrylate) nanocomposites. J Therm Anal Calorim. 2019;135:2159–69. https://doi.org/10.1007/s10973-018-7285-9.

10. Soleimani E, Niavarzi FB. Preparation, characterization and properties of PMMA/NiO polymer nanocomposites. J Mater Sci Mater Electron. 2018;29:2392–405. https://doi.org/10.1007/s10854-017-8158-x.

11. Sarkar S, Guibal E, Quignard F, SenGupt AK. Polymer-supported metals and metal oxide nanoparticles:synthesis, characterization, and applications. J Nanopart Res. 2012;14:715. https://doi.org/10.1007/s11051-011-0715-2.

12. Vavouraki AI, Gounaki I, Venieri D. Properties of inorganic polymers based on ground waste concrete containing CuO and ZnO nanoparticles. Polymers. 2021;13:2871. https://doi.org/10.3390/polym13172871.

13. Aldosari MA, Othman AA, Alsharaeh EH. Synthesis and characterization of the in-situ bulk polymerization of PMMA containing graphene sheets using microwave irradiation. Molecules. 2013;18(3):3152–67.

14. Nair PP, Rajan S, George KE. Insitu polymerisation of styrene using nano clay and optimization of strength using central composite design. Int J Eng Res Appl. 2012;2:1045–9.

15. Pirsa S, Zandi M, Almasi H, Hasanlu S. Selective hydrogen peroxide gas sensor based on nanosized polypyrrole modified by CuO nanoparticles. Sens Lett. 2015;13:1–6. https://doi.org/10.1166/sl.2015.3506.

16. Mishra SR, Ahmaruzzaman M. Cerium oxide and its nanocomposites: Structure, synthesis, and wastewater treatment applications. Mater Today Commun. 2021;28:102562. https://doi.org/10.1016/j.mtcomm.2021.102562.

17. Ramesan MT, Jayakrishnan P, Sampreeth T, Pradyumnan PP. Temperature-dependent AC electrical conductivity, thermal stability and different DC conductivity modelling of novel poly (vinyl cinnamate)/zinc oxide nanocomposites. J Therm Anal Calorim. 2017;129:135–45.

18. Suhailath K, Ramesan MT. Effect of neodymium-doped titanium dioxide nanoparticles on the structural, mechanical, and electrical properties of poly (butyl methacrylate) nanocomposites. J Vinyl Addt Technol. 2019;25:9–18. https://doi.org/10.1002/vnl.21673.

19. Ramesan MT. Dynamic mechanical properties, magnetic and electrical behavior of iron oxide/ethylene vinyl acetate nanocomposites. Polym Compos. 2014;35:1989–96. https://doi.org/10.1002/pc.22858.

20. Ramesan MT, Nushhat K, Parvathi K, Anilkumar T. Nickel oxide @ polyindole/phenothiazine blend nanocomposites: preparation, characterization, thermal, electrical properties and gas sensing applications. J Mater Sci Mater Electron. 2019;30:13719–28. https://doi.org/10.1007/s10854-019-01753-8.

21. Özgür U, Alivov YI, Liu C, Teke A, Reshchikov MA. A comprehensive review of ZnO materials and devices. J Appl Phys. 2005;98:041301. https://doi.org/10.1063/1.1992666.

22. Hamzah MQ, Mezan SO, Tuama AN, Jabbar AH, Agam MA. Study and characterization of polystyrene/titanium dioxide nanocomposites (PS/TiO$_2$ ncs) for photocatalytic degradation application: a review. Int J Eng Technol. 2018;7:538–43. https://doi.org/10.14419/IJET.V7I4.30.28172.

23. Abdelsayed V, Alsharaeh E, El-Shall MS. Catalyzed radical polymerization of styrene vapor on nanoparticle surfaces and the incorporation of metal and metal oxide nanoparticles within polystyrene polymers. J Phys Chem B. 2006;110:19100–3. https://doi.org/10.1021/jp064720p.

24. Motawie AM, Ahmed SM, et al. Physico mechanical properties of nano polystyrene nanocomposites. Egypt J Chem. 2017;60:261–76. https://doi.org/10.21608/ejchem.2017.2928.

25. Fang J, Xuan Y, Li Q. Preparation of polystyrene spheres in different particle sizes and assembly of the PS colloidal crystals. Sci China Technol Sci. 2010;53:3088–93. https://doi.org/10.1007/s11431-010-4110-5.

26. El-Din MRN, Hashem AI, Morsi RE, El-Azeim AA. New superhydrophobic nanocomposites as anti-corrosion coating films. Part I: Synthesis and characterization of poly (styrene/vinyl acetate)-SiO2 nanocomposites as a water repelling surface via nanoemulsion polymerization technique. J Mol Liq. 2021;322:114885. https://doi.org/10.1016/j.molliq.2020.114885.

27. Ramesan MT, Sankar S, Kalladi AJ, Abdulla ACL, Bahuleyan BK. Hydroxyapatite nanoparticles reinforced polyvinyl alcohol/chitosan blend for optical and energy storage applications. Polym Eng Sci. 2024;64:1378–90. https://doi.org/10.1002/pen.26623.

28. Tamuly C, Saikia I, Hazarikaa M, Das MR. Reduction of aromatic nitro compounds catalyzed by biogenic CuO nanoparticles. RSC Adv. 2014;4:53229–36. https://doi.org/10.1039/C4RA10397A.

29. Ramesan MT, Alex R. Compatibilization of SBR/NBR blends using chemically modified styrene-co-butadiene rubber Part 2. Effect of compatibilizer loading Polym Int. 2001;50:1298–308. https://doi.org/10.1002/pi.775.

30. Kandulna R, Choudhary RB, Singh R, Purty B. PMMA–TiO$_2$ based polymeric nanocomposite material for electron transport layer in OLED application. J Mater Sci: Mater Electron. 2018;29:5893–907. https://doi.org/10.1007/s10854-018-8562-x.

31. Ismail MS, Elamin AA, Abdel-Wahab F, Elbashar YH, Mahasen MM. Improving the refractive index by engineering PbS/PVA nano polymer composite for optoelectronic applications. Opt Mater. 2022;131:112639. https://doi.org/10.1016/j.optmat.2022.112639.

32. Ramesan MT, Nidhisha V, Jayakrishnan P. Facile synthesis, characterization and material properties of a novel poly (vinyl cinnamate)/nickel oxide nanocomposite. Polym Int. 2017;66:548–56. https://doi.org/10.1002/pi.5288.

33. Hassan D, Ah-yasari AH. Fabrication and studying the dielectric properties of (polystyrene-copper oxide) nanocomposites for piezoelectric application. Bull Electr Eng Inform. 2019;8:52–7. https://doi.org/10.11591/eei.

34. Jayakrishnan P, Ramesan MT. Temperature dependence of the electrical conductivity of poly (anthranilic acid)/magnetite nanocomposites and the applicability of different conductivity models. Polym Compos. 2018;39:2791–800. https://doi.org/10.1002/pc.24271.